www.czasopisma.pan.pl PAN POLSKA AKADEMIA NAUK www.journals.pan.pl

Arch. Metall. Mater. **64** (2019), 4, 1377-1384

DOI: 10.24425/amm.2019.130104

A.GOŁDASZ*#, Z. MALINOWSKI*, A. CEBO-RUDNICKA*

THERMOMECHANICAL ANALYSIS OF THE CHARGE HEATING IN A ROTARY FURNACE

This paper presents the methodology for determining thermal strains and stresses during heating the charge in a rotary furnace. The calculations were made with the original software, which uses the finite element method. The heat transfer boundary conditions used for computing were verified on the basis of industrial tests. Good compatibility between the experimental data and numerical calculations was obtained. The possibility of the material cracking occurrence was checked for a set exhaust gas temperature distribution on the furnace length. As a result, it was possible to develop steel heating curves characterized by short process times.

Keywords: charge heating, heating curves, thermal stresses

1. Introduction

The primary objective of the charge heating process in heating furnaces is to obtain an appropriate temperature distribution in the material cross-section. However, excessively fast heating of the material can lead to its high susceptibility to cracking. The number of factors which can contribute to the formation of thermal stresses is very high and, therefore, the determination of thermal stresses is a very complicated task. During charge heating, the formation of thermal stresses is primarily caused by a non-uniform charge temperature field and the steel phase transitions occurring in the solid state. To be able to determine thermal stresses, first the temperature field of the heated charge must be established. The temperature distribution in the charge during the heating process is influenced by the boundary conditions of the heating process and the thermo-physical properties of the charge, which in turn depend on the steel grade of the heated material [1].

The boundary conditions are determined with direct and indirect methods. For direct methods, classic equations describing basic heat transfer mechanisms are solved. For indirect methods, we measure a characteristic parameter, e.g. the temperature distribution during an actual process (in industrial or laboratory conditions), and we use it as the basis for determining the amount of heat reaching the surface [2].

The Heiligenstaedt [3] model is often used to describe the heat exchange in heating furnace chambers, assuming that we know the temperatures of exhaust gas, furnace wall surfaces and the charge. Based upon the furnace measurement systems, the resultant heat fluxes reaching the charge surface are determined with more or less simplified methods. This methodology was applied in the paper [4] in order to build a model of the pusher furnace thermal operation control. The temperature of the exhaust gas from the combustion of natural gas, resulting from a simplified furnace model, was the control parameter. This model is an effect of the earlier studies of the Authors on the heat exchange in continuous furnaces [5-6]. In addition, models based on balance equations describing the heat exchange in individual furnace zones are widely used [7-8]. The brightness method is also commonly used due to its simplicity in connection with the zone method [9]. In this method, the radiation energy stream is determined by relating the furnace wall temperature to the furnace atmosphere temperature, which leads to a significant simplification of calculations and, consequently, a very effective numerical model is obtained, allowing the charge heating curves to be developed. However, this model needs to be verified on a one-off basis by measuring the charge and furnace atmosphere temperature. The methods presented hereinabove are more or less simplified. To obtain an accurate solution, methods for describing the radiation energy flow in the furnace chamber need to be applied and coupled with the solution of the thermal conductivity equation in the material heated, and the exhaust gas velocity distribution and exhaust gas composition must be known. A detailed description of methods for describing the radiation heat transfer can be found in [10]. Unfortunately, they usually feature a prolonged computing time.

During heating steel in rotary furnaces, a non-uniform temperature field forms within the material, contributing to the formation of thermal stresses. In addition, changes in the steel volume caused by allotropic transformations in the solid state affect the formation of stresses in the material heated.

* AGH UNIVERSITY OF SCIENCE AND TECHNOLOGY, FACULTY OF METALS ENGINEERING AND INDUSTRIAL COMPUTER SCIENCE, AL. MICKIEWICZA 30, 30-059 KRAKOW, POLAND

Corresponding author: andrzej.goldasz@agh.edu.pl

During heating, a small dimension charge, the probability of the occurrence of stresses, which could lead to charge cracking, is low. However, an unequivocal certainty as regards the applied heating rate, and whether it is correct or not, can be acquired by the analysis of information concerning the maximum thermal strains and the mean stress. Fracture mechanics [11] offers a number of possibilities for determining the boundary conditions leading to a material failure. In particular, cast materials having a non-uniform structure, voids, porosities, inclusions and other phase particles, have a limited resistance to cracking. The authors of the paper [12] indicate that the fracture criterion based upon boundary strain taking into account the influence of mean stress must be applied to assess the possibility for crack occurrence.

2. The heat transfer model

The determination of the temperature field of the bloom heated requires solving a heat transfer problem between the exhaust gas – the furnace chamber and the charge heated. Due to the position of the charge on the refractory bottom, it is assumed that there is no heating and no heat losses between the charge and the refractory bottom. The temperature field of the bloom heated will be determined from the heat conduction equation, which in Cartesian coordinates assumes the form [13]:

$$\frac{\partial T}{\partial \tau}=\frac{1}{\rho c}\left[\frac{\partial}{\partial x_1}\lambda\left(\frac{\partial T}{\partial x_1}\right)+\frac{\partial}{\partial x_2}\lambda\left(\frac{\partial T}{\partial x_2}\right)+\frac{\partial}{\partial x_3}\lambda\left(\frac{\partial T}{\partial x_3}\right)\right]+\frac{q_v}{\rho c} \quad (1)$$

where:

λ – thermal conductivity, W/(m×K);
x_1, x_2, x_3 – Cartesian coordinates, m;
ρ – density, kg/m^3;
c_p – specific heat, J/(k×gK);
q_v – capacity of the external heat source, W/m^3;
τ – time, s.

The temperature field $T(x,y,z,\tau)$ resulting from the solution of the equation (1) should satisfy the boundary conditions on the surface of the material heated:

$$\dot{q}_w\left(S_w,\tau\right)=\alpha_e\left(S_w,\tau\right)\left[T_w\left(S_w,\tau\right)-T_g\left(\tau\right)\right] \quad (2)$$

where:

α_e – effective heat transfer coefficient, W/(m^2×K);
T_w – temperature of the charge surface S_w fanned by exhaust gas, K;
T_g – exhaust gas temperature, K.

The finite element method was applied to solve the heat conduction equation, in accordance with the methodology described in detail in [1]. The Galerkin integration scheme and linear shape functions were used.

To determine the temperature field of the bloom heated in the rotary furnace, the boundary conditions of heat transfer on the surface of the charge heated need to be established. A simplified model was applied to describe the heat transfer within the furnace chamber, in which the furnace chamber, at a specific time τ, is treated as a closed system consisting of two isothermal surfaces and an isothermal gas body, Fig. 1.

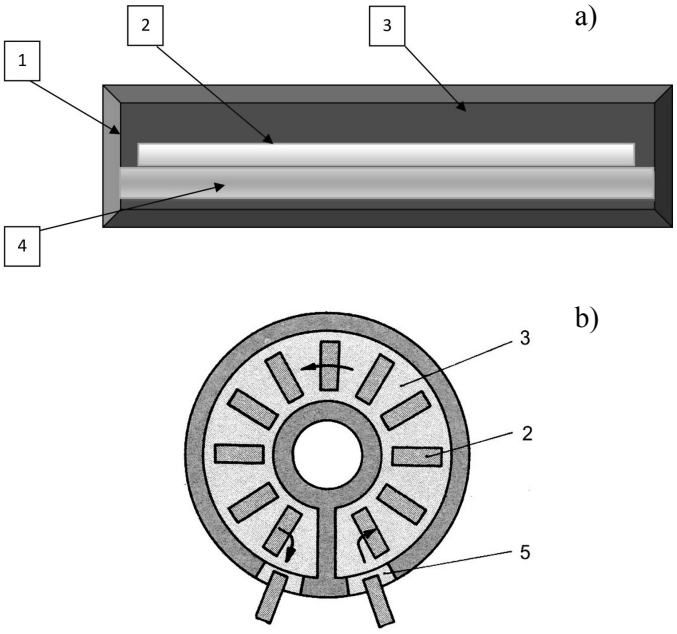

Fig. 1. Rotary furnace: a) chamber cross-section; b) diagram: 1 – Furnace walls and roof (F_1); 2 – Slab heated (F_2); 3 – Flue gas; 4 – Rotary bottom; 5 – Inlet

Isothermal surfaces are the charge surface F_2 and the furnace chamber surface F_1. The model assumes that the density of the gas emissions reaching both surfaces is the same and the transparency of the gas body 3 on the slab surface is the same. The mean density of heat flux absorbed by the bloom surface was determined as the sum of the gas body radiation flux, the heat convection flux resulting from the exhaust gas movement and the flux of furnace chamber radiation on the bloom surface.

$$\dot{q}_w=\propto_{gw}\left(T_g-T_w\right)+\varepsilon_g\varepsilon_w 5.67\cdot10^{-8}\left(T_g^4-T_w^4\right)+$$
$$+\varepsilon_{sw}P_g\,5.67\cdot10^{-8}\left(T_1^4-T_w^4\right) \quad (3)$$

where:

ε_g – gas body emissivity;
ε_w – bloom surface emissivity;
ε_{sw} – substitute emissivity of the wall-charge system;
P_g – gas body transparency for radiation on the bloom surface;
α_{gw} – coefficient of convective heat transfer on the bloom surface;
T_g – gas body temperature, K;
T_1 – furnace chamber surface temperature, K;
T_w – bloom surface temperature, K.

In equation (3), the density of exhaust gas body radiation was computed using the Hottel's gas model [10]. The forced convection conditions were taken into account for determining the Nusselt number and the convective heat transfer coefficient. The furnace wall temperature T_1 was determined on the basis of the exhaust gas temperature [9].

3. Thermal stress model

Thermal stresses can be established after determining the temperature field. Thermal strains were computed with the finite element method using the methodology described in the paper [1]. As plastic deformations can occur within the material, especially when thermal expansion, which is caused by phase transitions, is taken into account, the stress field is determined with the incremental method. Relationships between the increments of stresses and strains were determined on the basis of the Prandtl-Reuss equations:

$$\Delta\sigma_{ij} = \frac{E}{1+\nu}\Delta\varepsilon_{ij} + \delta_{ij}\frac{\nu E}{(1+\nu)(1-2\nu)}\Delta\varepsilon_{kk} + \\ - \frac{3}{2}\varphi\frac{\Delta\varepsilon_{kl}s_{kl}}{\sigma_p^2\left(1+\frac{H_p}{3G}\right)}\varepsilon_{ij} \tag{4}$$

where:

E – Young's modulus, Pa
ν – Poisson's ration
σ_p – flow stress, Pa
H_p – plastic modulus, Pa
G – shear modulus, Pa
δ_{ij} – Kronecker delta.

In equation (4) for the plastic state variable $\varphi = 1$. However, in the elastic loading or unloading range $\varphi = 0$, and the equation is reduced to the equations of the linear theory of elasticity. In the thermal stress model, it is necessary to limit the values of stresses calculated from the equations of the theory of elasticity to the yield point. After reaching the yield point, the further increase in the stress is proportional to the plastic modulus H_p, and not to the Young's modulus E. Therefore, it is necessary to determine the approximate value of the yield point and the value of plastic modulus H_p. The yield stress and the value of plastic modulus were determined from the Shida formulas [14] on the basis of carbon content and the temperature. The method of structure changes resulting from the charge heating and their influence on the state of strains and stresses is taken into consideration by changes in the Young's modulus, Poisson's coefficient and the coefficient of thermal expansion (Fig. 5). The method of transferring the impact of structural changes through these parameters is described in the paper [1].

The fracture criterion based upon the boundary strain taking into account the influence of the mean stress was applied [12] to assess the possibility of crack occurrence.

$$\begin{aligned} \bar{\varphi}_f &= \sum\Delta e_i \quad \text{for } \sigma_m > 0 \\ \bar{\varphi}_f &= 0 \quad\quad\;\; \text{for } \sigma_m < 0 \end{aligned} \tag{5}$$

The criterion (5) anticipates the material failure at the time when the sum of increments of thermal effective strain Δe_i exceeds the value of effective strain $\bar{\varphi}_f$ determined in the bloom material uniaxial tensile test. For blooms from the continuous casting, the parameter $\bar{\varphi}_f$ should not exceed the value of 0.04 at the spots where the mean stress is positive.

4. Charge heating model validation

The formulated heat transfer model of charge heating in a rotary furnace was verified by comparing the temperature measurements acquired during heating a test bloom with the cross-section 270×320 mm and the measurement part length of 1500 mm by using the Datapaq Slab Reheat system. While heating the bloom, the furnace atmosphere temperature was measured, and the bloom temperature at a depth of 30 mm from the bottom face and 30 mm from the top face and on the bloom axis. Fig. 2 shows a comparison of the computing results with the data acquired from the measurements for the bloom axis. The differences are insignificant and confirm the satisfactory compatibility of the charge heating model with the measurements. For a set furnace temperature and rotation time, the bloom temperature changes are correctly reflected. The equalising of the bloom temperature on the solid bottom enabled an almost identical temperature to be achieved in the whole cross-section of the bloom, and this temperature was about 1258°C upon the completion of heating, Fig. 3.

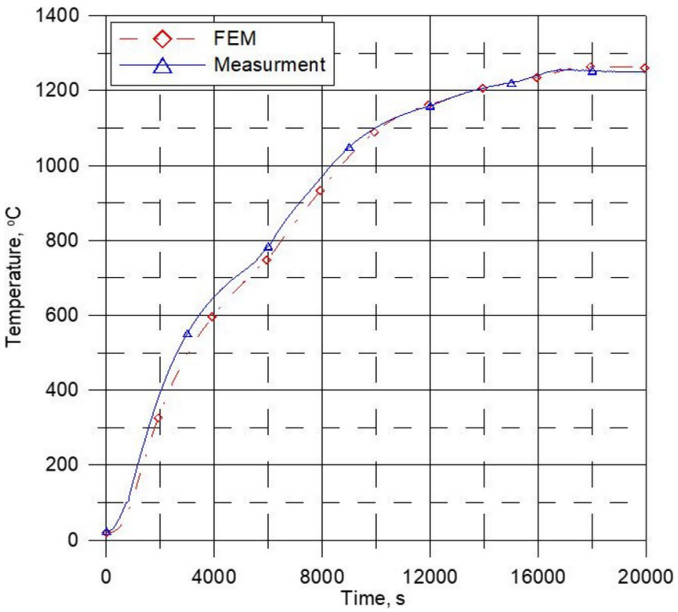

Fig. 2. Comparison of the computing results of the temperature on the test bloom axis with the measurement data

5. Numerical computing

Computing the temperature distribution and the stress and strain fields was carried out for the heating process of steel 1.7174 in a rotary furnace. The heating time was 235 minutes and the maximum exhaust gas temperature in the heating zone was 1210°C, whereas in the equalising zone it was 1200°C. This is the time to obtain a charge temperature distribution suitable for rolling. Steel properties are shown in Figs. 4 and 5.

Figs. 6 and 8 present the distribution of logarithmic strain caused by thermal stresses in the axis and on the surface of the charge, after 30 minutes and 235 minutes, respectively, or on

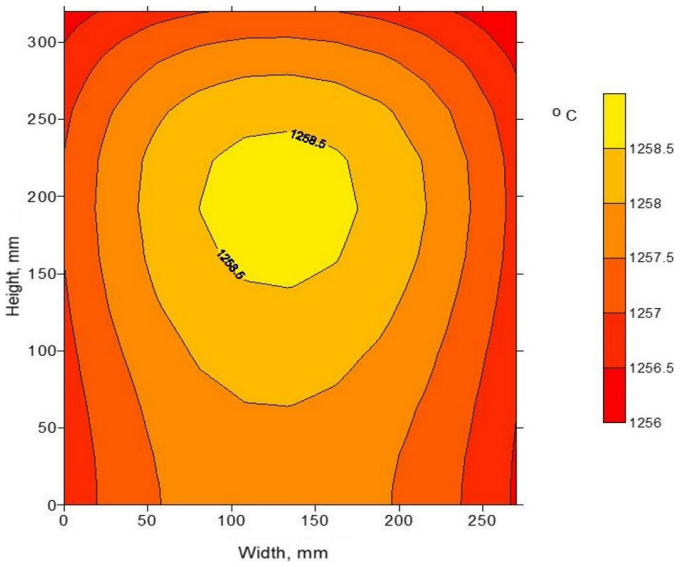

Fig. 3. The temperature distribution in the cross-section of the test bloom after the completion of the heating

completion of the heating process. The logarithmic strain achieves its highest values on the bloom surface, where the effective strain after 30 minutes heating is about 0.004. However, after the completion of the heating process, the maximum value of logarithmic effective strain on the charge surface does not exceed 0.02. The intensity of the logarithmic strain on the bloom axis is even lower, although its growth during heating can be observed. After 30 minutes of the heating process, the value of logarithmic effective strain does not exceed 0.001, and on completion of the heating process it is about 0.005. Figs. 7 and 9 show a change in the stress triaxiality factor in the axis and on the bloom surface, after 30 minutes and on completion of the heating process. The obtained computing results indicate that during the whole heating process, the ratio of the mean stress to the effective stress along the whole length of the charge, on the bloom surface and on its axis is negative. This fact, along with the information on the value of logarithmic effective strain, which during the whole heating process is below the critical value of 0.04, indicates that compression stresses prevail in the bloom heated, and the probability of crack development is low.

Figs. 10a and b present the temperature field within the charge after 30 minutes and on the completion of heating. The obtained calculation results present a symmetrical temperature distribution in the bloom heated, which results from adopting symmetrical boundary conditions for heat transfer on the surface of the charge heated applied to describe the heat conduction during the bloom heating process. On the completion of heating, we can find that the temperature field in the material heated is almost even (Fig. 10b). The maximum temperature difference occurring in the charge on the completion of heating is small and it is approx. 7°C.

The calculation results presenting the mean stress distribution in the charge after 30 minutes of heating (Fig. 11a) show a negative value of the mean stress in the whole bloom

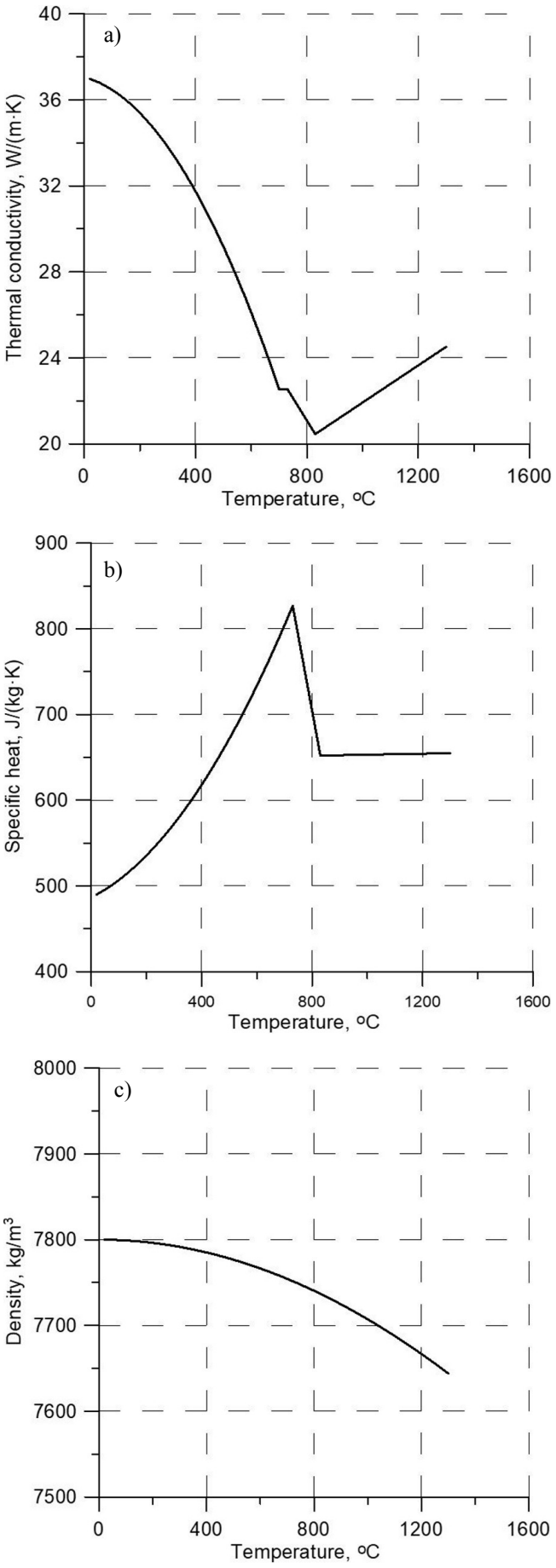

Fig. 4. Thermal properties of the steel analysed: a) heat conduction coefficient; b) specific heat; c) density

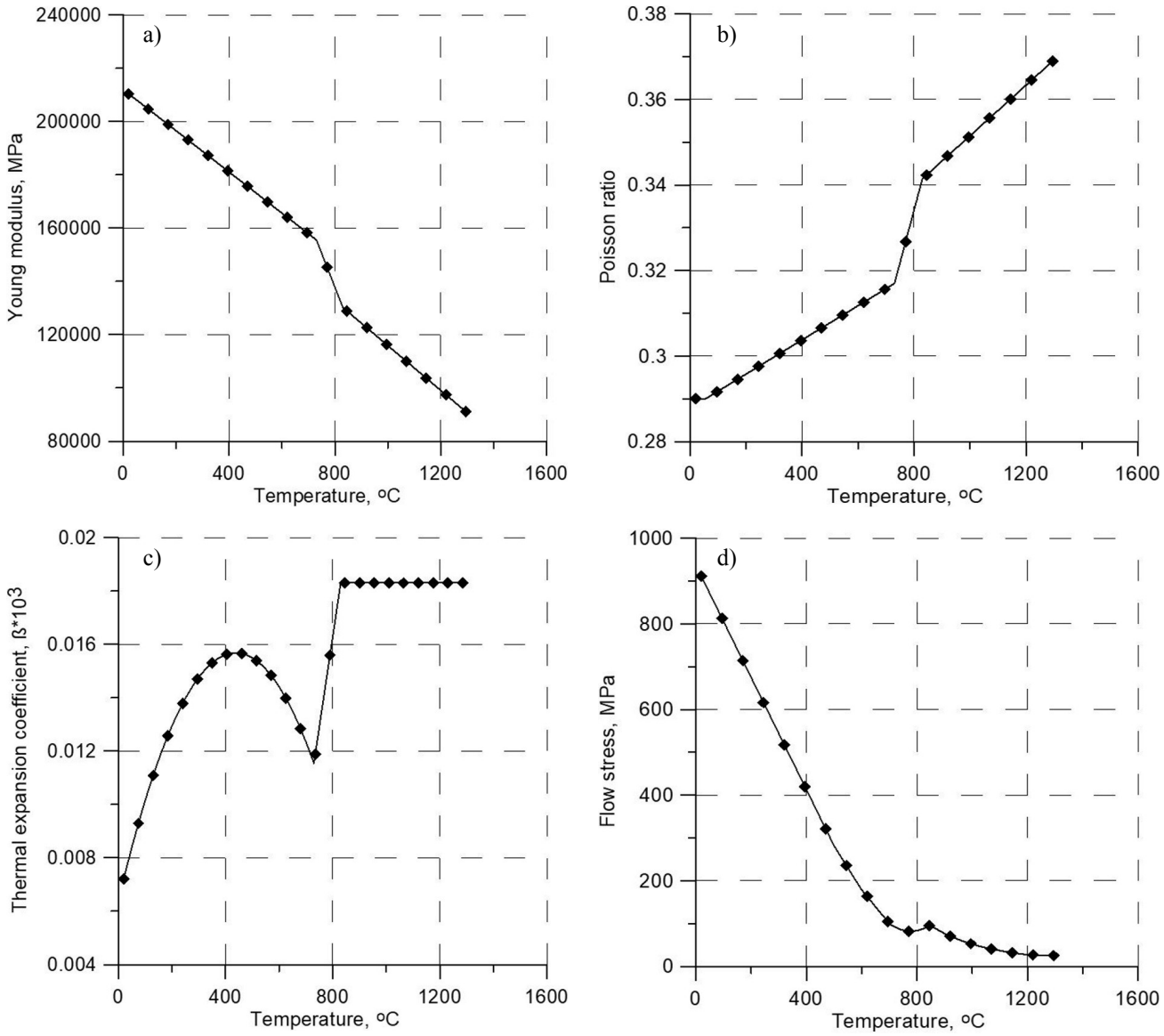

Fig. 5. Mechanical properties of the steel analysed: a) Young's modulus; b) Poisson's ratio, c) linear expansion; d) yield stress

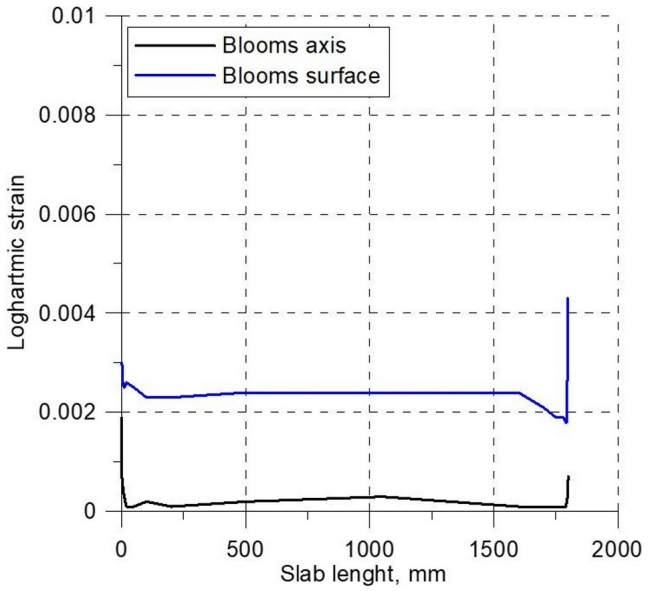

Fig. 6. Distribution of logarithmic strain in the axis and on the charge surface after 30 minutes of heating

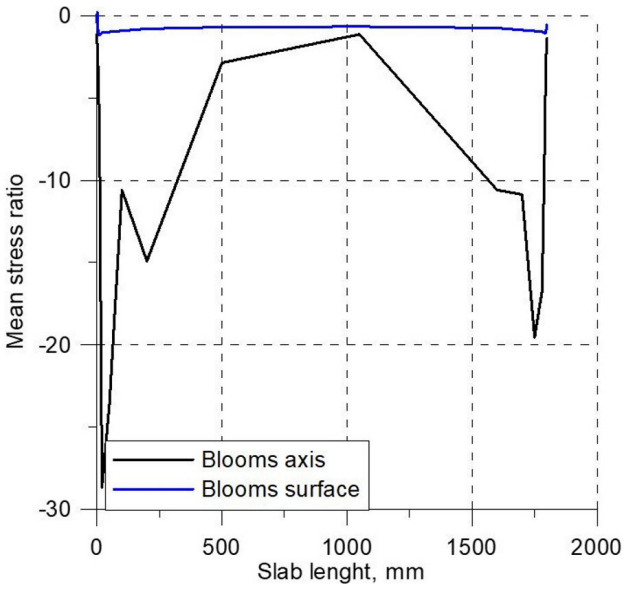

Fig. 7. Ratio of mean stress to effective stress in the axis and on the charge surface after 30 minutes of heating

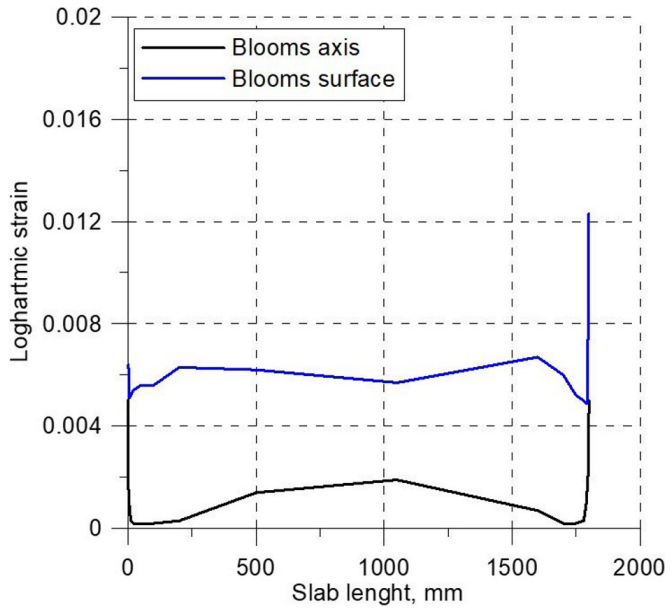

Fig. 8. Distribution of logarithmic strain in the axis and on the charge surface on the completion of heating

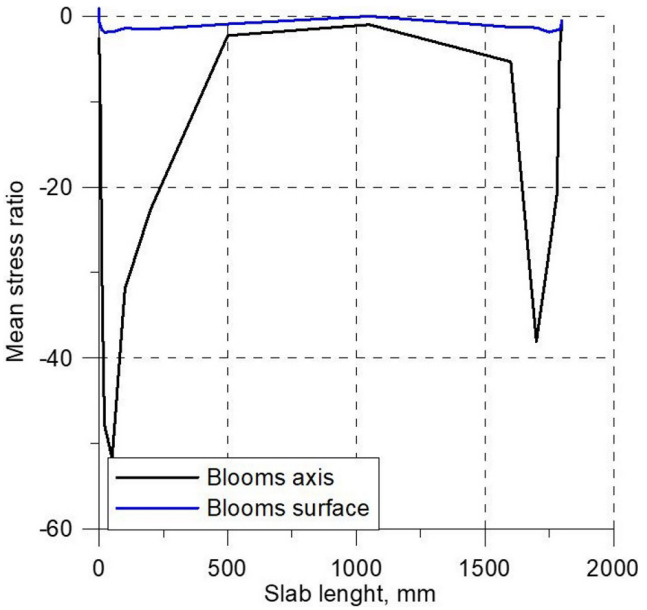

Fig. 9. Ratio of mean stress to the effective stress in the axis and on the charge surface on the completion of heating

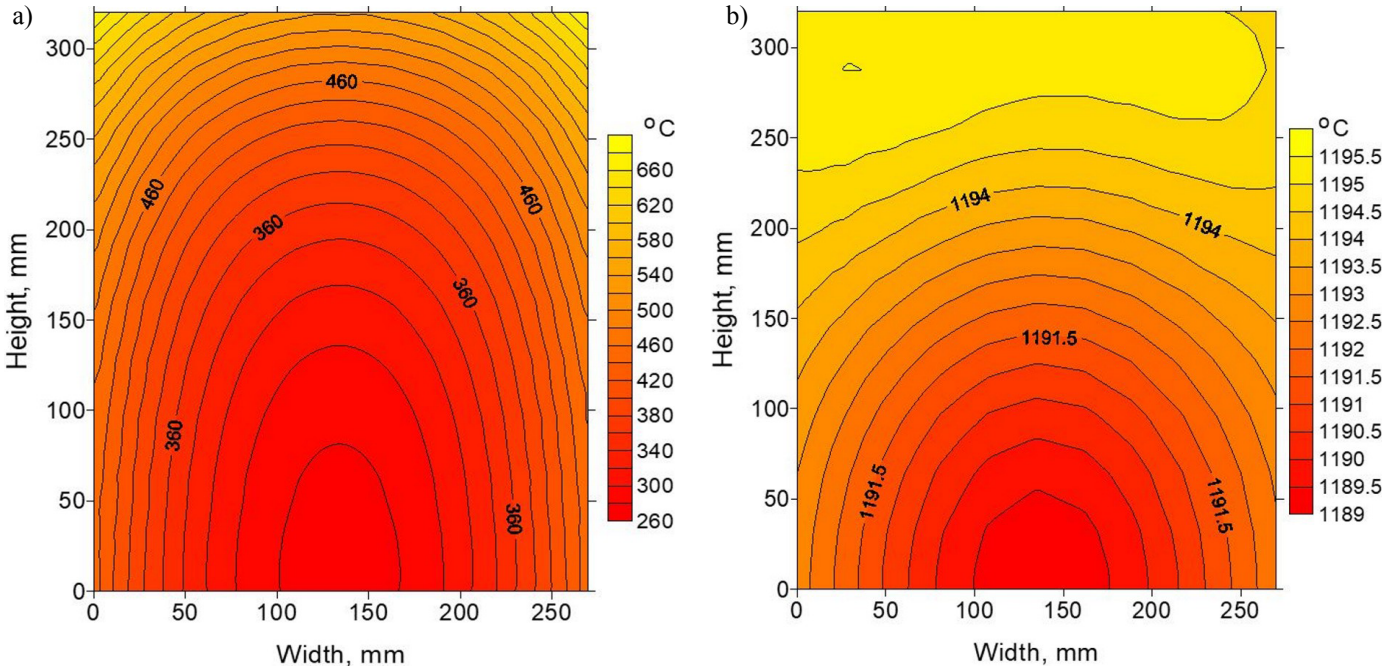

Fig. 10. The charge temperature distribution after 30 minutes (a) and on the completion (b) of heating

cross-section, which is on average –100 MPa, and indicates the existence of compression stress. However, on the completion of heating (Fig. 11b), one can observe the small positive values of the mean stress, below 5 MPa, which appear around the charge corners.

The distribution of effective strain in the charge cross-section after 30 minutes of heating confirms that the maximum value of effective strain does not exceed 0.004, both in the bloom axis, and on its surface, only at the charge corners a small increase in the value of this parameter up to approx. 0.005 can be observed (Fig. 12a). Upon the completion of heating, the effective strain in the whole bloom cross-section is approx. 0.004, whereas in the corners one can observe its increase to approx. 0.02 (Fig. 12b).

6. Conclusion

The numerical calculations, carried out to optimize the time of charge heating, allow us to determine the heating curve that insures the specified quality of the material without thermal cracks. This is confirmed by very low values of logarithmic effective strain, which for none of the steels considered, during

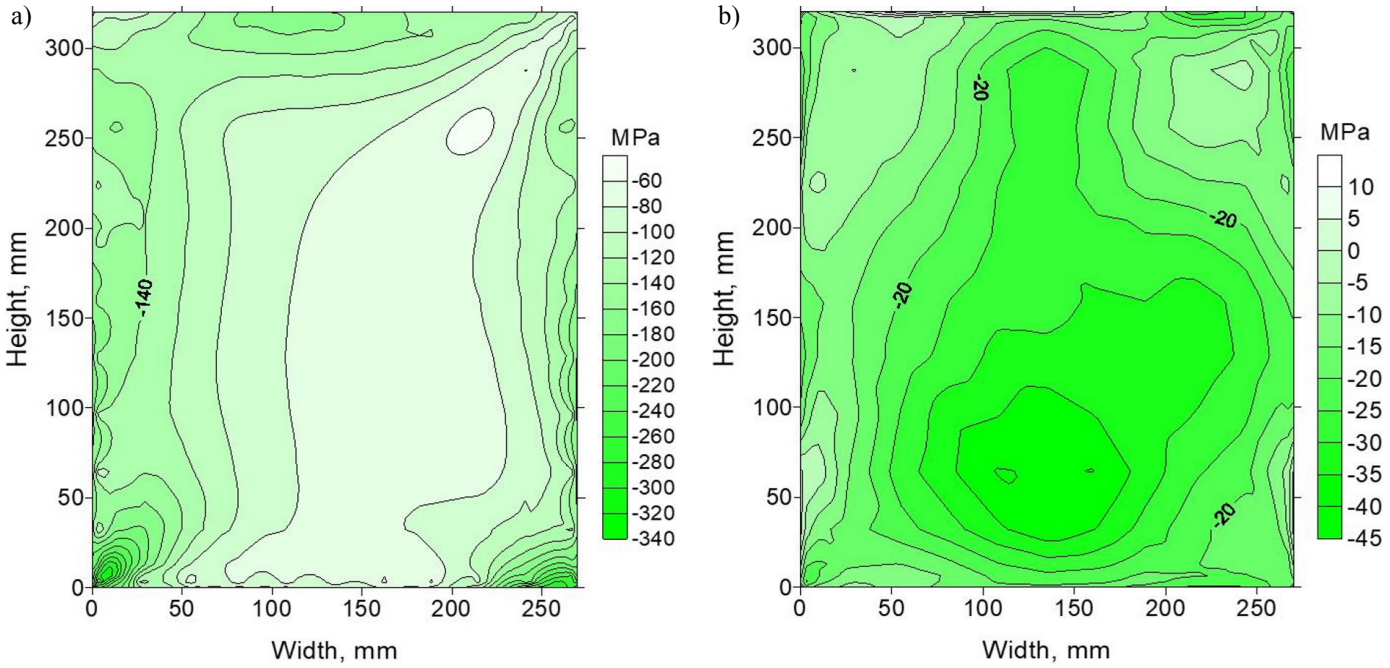

Fig. 11. Mean stress distribution in the charge after 30 minutes (a) and on the completion (b) of heating

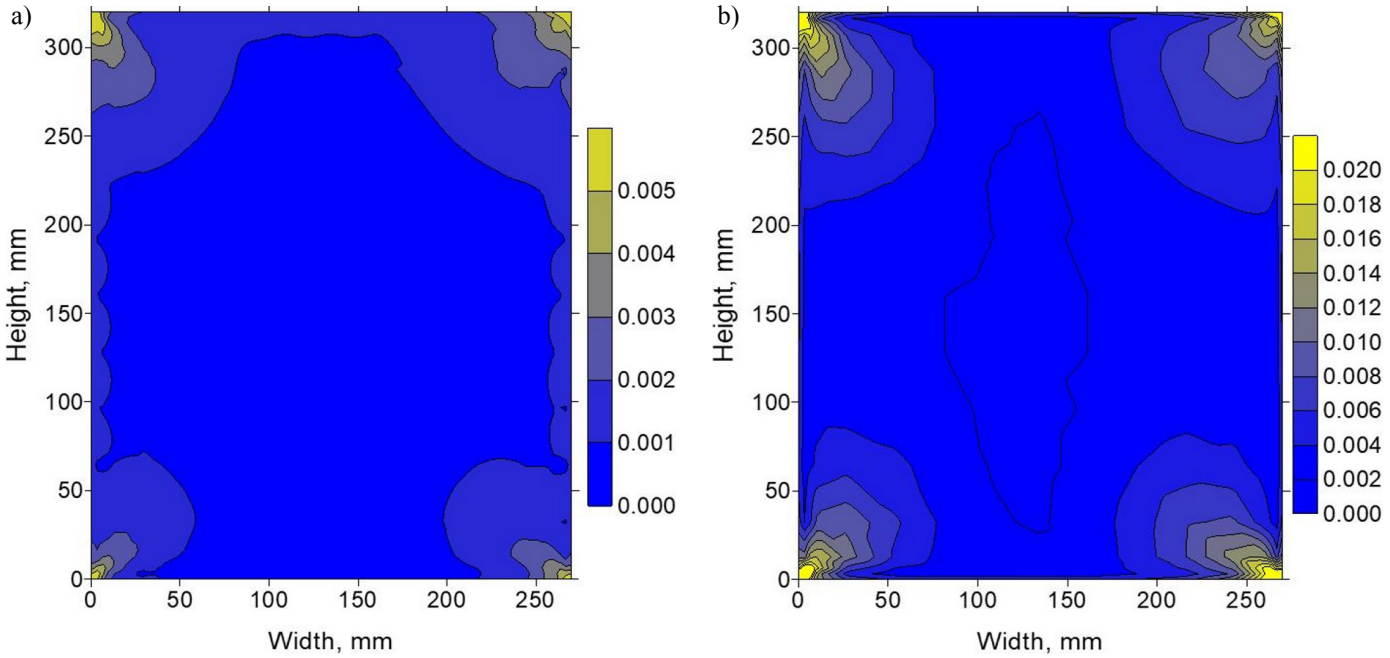

Fig. 12. Distribution of effective logarithmic strain in the charge after 30 minutes (a) and on the completion (b) of heating

the whole heating process, exceeded their critical value, which for continuously cast blooms is approx. 0.04.

The temperature distribution in the charge heated upon the completion of the heating process is almost uniform, and the smallest difference between the minimum and maximum temperature inside the charge heated on the completion of heating is 7°C. The methodology of the determination of thermal strains and stresses presented in this paper can be successfully applied for developing new heating curves. When it is applied, it will be possible to check the possibilities for material cracking even at the most intensive process of charge heating.

Final remark

Scientific study financed from the regular activity of the Faculty of Metals Engineering and Industrial Computer Science of AGH University of Science and Technology, Work no. 16.16.110.663.

REFERENCES

[1] Z. Malinowski Zbigniew, Numeryczne modele w przeróbce plastycznej i wymianie ciepła, Kraków 2005.

[2] A. Gołdasz, Identyfikacja warunków brzegowych wymiany ciepła w komorach pieców grzewczych, Kraków 2017.

[3] W. Heiligenstaedt, Wärmetechnische Rechnungen für Industrieöfen, Düsseldorf 1996.

[4] A. Jaklic, F. Vode, T. Kolenko, Applied Thermal Engineering **27**, 1105-1114 (2007).

[5] A. Jaklic, B. Glogovac, T. Kolenko, B. Zupancic, B. Tezak, Applied Thermal Engineering **22**, 873-883 (2002).

[6] A. Jaklic, T. Kolenko, B. Glogovac, Applied Thermal Engineering **25**, 793-795 (2005).

[7] P. Gruszka, Z. Rudnicki, Archiwum Hutnictwa **21** (4), 613-631, (1976).

[8] J. Nadziakiewicz, Z. Rudnicki, Archiwum Hutnictwa **26** (4), 637-649 (1981).

[9] A. Gołdasz, Z. Malinowski, T. Telejko, M. Rywotycki, A. Szajding, Archives of Metallurgy and Materials **57** (4), 1143-1149 (2012).

[10] J. Howell, R. Siegel, P. Menguc, Thermal Radiation Heat Transfer, CRC Press 2011.

[11] B. Dodd, Y. Bai, Ductile Fracture and Ductility, London 1987.

[12] A. Cebo-Rudnicka, Z. Malinowski, T. Telejko, Archives of Metallurgy and Materials **62** (2), 459-471 (2017).

[13] Y.A. Cengel, Heat Transfer A Practical Approach 3rd edition, McGraw-Hill 2007.

[14] S. Shida, Effect of carbon content, temperature and strain rate on compressive flow stress of carbon steel, Hitachi Res. Lab. Report, 1-19 (1974).